LJMU Research Online

Mucciarelli, A, Lapenna, E, Massari, D, Pancino, E, Stetson, PB, Ferraro, FR, Lanzoni, B and Lardo, C

 A Chemical Trompe-L'ceil: No Iron Spread In The Globular Cluster M22

http://researchonline.ljmu.ac.uk/id/eprint/4841/

Article

A chemical *trompe-l'œil*: no iron spread in the globular cluster M22 [1]

A. Mucciarelli[2], E. Lapenna[2], D. Massari[3,4], E. Pancino[3], P.B. Stetson[5], F.R. Ferraro[2], B. Lanzoni[2], C. Lardo[6]

[2]*Dipartimento di Fisica & Astronomia, Università degli Studi di Bologna, Viale Berti Pichat, 6/2 - 40127 Bologna, Italy*

[3]*INAF - Osservatorio Astronomico di Bologna, Via Ranzani 1 - 40127 Bologna, Italy*

[4]*Kepteyn Astronomical Institute, University of Groningen, Landleven 12, 9747 AD Groningen, The Nethelands*

[5]*National Research Council, 5071 West Saanich Road, Victoria, BC V9E 2E7, Canada*

[6]*Astrophysics Research Institute, Liverpool John Moores University, 146 Brownlow Hill, Liverpool L3 5RF, United Kingdom*

ABSTRACT

We present the analysis of high-resolution spectra obtained with UVES and UVES-FLAMES at the Very Large Telescope of 17 giants in the globular cluster M22, a stellar system suspected to have an intrinsic spread in the iron abundance. We find that when surface gravities are derived spectroscopically (by imposing to obtain the same iron abundance from FeI and FeII lines) the [Fe/H] distribution spans ∼0.5 dex, according to previous analyses. However, the gravities obtained in this way correspond to unrealistic low stellar masses (0.1-0.5 $M_\odot$) for most of the surveyed giants. Instead, when photometric gravities are adopted, the [FeII/H] distribution shows no evidence of spread at variance with the [FeI/H] distribution. This difference has been recently observed in other clusters and could be due to non-local thermodynamical equilibrium effects driven by over-ionization mechanisms, that mainly affect the neutral species (thus providing lower [FeI/H]) but leave [FeII/H] unaltered. We confirm that the s-process elements show significant star-to-star variations and their abundances appear to be correlated with the difference between [FeI/H] and [FeII/H]. This puzzling finding suggests that the peculiar chemical composition of some cluster stars may be related to effects able to spuriously decrease [FeI/H]. We conclude that M22 is a globular cluster with no evidence of intrinsic iron spread, ruling out that it has retained the supernovae ejecta in its gravitational potential well.

1.   Introduction

In the last decade, the investigation of the properties of the globular clusters (GCs) and their possible departures from the canonical paradigm of simple stellar population has become a hot astrophysical topic. The general homogeneity in the Fe content measured in most of them (see e.g. Carretta et al. 2009a) is considered as the typical feature to distinguish GCs from more complex stellar systems (Willman & Strader 2012), suggesting that in the past GCs were not massive enough to retain the ejecta of supernovae (SNe) in their gravitational well. On the other hand, the intrinsic star-to-star variations in the elements involved in the proton capture processes (the high temperature extension of the CNO-cycle) observed in all the old and massive GCs (see e.g. Mucciarelli et al. 2009; Carretta et al. 2009b; Larsen et al. 2014) suggest that these systems have been able to retain low-energy ejecta, possibly synthesized in asymptotic giant branch (AGB), fast-rotating massive and/or binary stars (see e.g. Decressin et al. 2007; D'Ercole et al. 2008; De Mink et al. 2009; Bastian et al. 2013; Denissenkov & Hartwick 2014). However, for a few GC-like systems an intrinsic iron spread has been detected, suggesting that those systems were able to retain the SN ejecta. The two undeniable cases are ω Centauri (Origlia et al. 2003; Johnson & Pilachowski 2010; Pancino et al. 2011; Marino et al. 2011a) and Terzan 5 (Ferraro et al. 2009; Origlia et al. 2011, 2013; Massari et al. 2014), both showing a 1 dex wide (and multi-modal) metallicity distribution. Significant intrinsic iron spreads (smaller than those of ω Centauri and Terzan 5) have been measured from high-resolution spectra in M54 (Carretta et al. 2010a), M22 (Marino et al. 2009, hereafter M09), M2 (Yong et al. 2014) and NGC 5286 (Marino et al. 2015). Other clusters have been proposed to have small intrinsic spreads but without conclusive results (see e.g. the case of NGC 1851, Carretta et al. 2010b).

Indeed, the analysis of GCs suspected to have an intrinsic Fe spread deserves a particular care. Recently, the Fe spreads previously measured in two GCs turned out to be spurious and due to unaccounted effects. In particular, in NGC 2419 the (spurious) evidence of an iron spread measured from the Ca II triplet by Cohen et al. (2010) and Ibata et al. (2011) is due to the peculiar chemical composition of the cluster (with a strong Mg depletion), which modifies the strength of the Ca II triplet lines (Mucciarelli et al. 2012). In NGC 3201 the detection of iron spread by Simmerer et al. (2013) is due to the inclusion of AGB stars in their sample, having [Fe/H] abundances systematically lower than those measured in red giant branch (RGB) stars (Mucciarelli et al. 2015). The observed effect has been suggested to be due to non-local thermodynamical equilibrium (NLTE) effects that affect mainly the

---

[1]Based on observations collected at the ESO-VLT under programs 068.D-0332, 071.D-0217 and 073.D-0211.

neutral species, lowering the abundance derived from FeI lines but leaving the abundances from FeII lines unaltered. A similar behavior has been observed also in AGB stars in M5 (Ivans et al. 2001) and 47 Tucanae (Lapenna et al. 2014).

Because of these recent results questioning previous claims of iron spread in some GCs, here we reanalyse the case of M22. This metal-poor GC is suspected to have an intrinsic Fe spread since forty years, because of the broad colour distribution of RGB observed in its color-magnitude diagram (CMD). However, the presence of differential reddening in the direction of M22 makes difficult to properly assess whether the observed color broadening is caused by an intrinsic metal spread (Monaco et al. 2004). From a spectroscopic point of view, conflicting results have been obtained based on small samples of stars (Cohen 1981; Pilachowski et al. 1982; Gratton 1982). Recently, M09 and Marino et al. (2011b) analysed high-resolution spectra of 35 giant stars finding that M22 harbors at least two groups of stars characterized by different iron, C+N+O and s-process element abundances: the first group has [Fe/H]=– 1.82 dex, [(C+N+O)/Fe]=+0.28 dex and solar-scaled [s/Fe] abundance ratios, while the second group has [Fe/H]=–1.67 dex, [(C+N+O)/Fe]=+0.41 dex and [s/Fe]∼+0.3/+0.4 dex. Of course, this result puts M22 on a different framework with respect to genuine GCs, suggesting that M22 retained not only s-process and CNO-cycle elements (which are typical high-mass AGB ejecta) but also the SNe ejecta.

In this paper, we present a new analysis of the sample of 17 giant stars of M22 that M09 used to provide the first evidence in support to an intrinsic metallicity spread in this cluster.

2. Observations

The spectroscopic dataset analysed here is the same used by M09 and includes six giant stars observed with UVES@VLT (Dekker et al. 2000) on 18-21 March 2002, and 11 giant stars observed with UVES-FLAMES@VLT (Pasquini et al. 2000) on 24-26 May 2003, adopting the Red Arm 580 grating that ranges from ∼4800 to ∼6800 Å with a typical spectral resolution R= 47000. All the spectra have been reduced with the dedicated ESO pipelines, including bias subtraction, flat-fielding, wavelength calibration, spectral extraction and order merging. The typical signal-to-noise ratio per pixel of the acquired spectra is ∼150 at ∼6000 Å.

The target stars, originally selected from the photometric catalog by Monaco et al. (2004), have been cross-identified in the UBVI ground-based catalog described in Kunder et al. (2013) and in the JHK_s 2MASS catalog (Skrutskie et al. 2006). Their position in the (V,B-V)

CMD is shown in Fig. 1. Main information about the targets is available in M09.

For each target the correction for differential reddening has been derived as in Milone et al. (2012), adopting the extinction law by Cardelli, Clayton & Mathis (1989). We found that the maximum variation of E(B-V) across the area covered by the observed targets is of $\sim$0.07 mag, in nice agreement with Monaco et al. (2004) who quoted a maximum variation of $\sim$0.06 mag. The true distance modulus, $(m - M)_0$= 12.65 mag, and the color excess, E(B-V)= 0.34 mag, of the cluster have been estimated by fitting the CMD with an isochrone from the BaSTI dataset (Pietrinferni et al. 2006), computed with an age of 12 Gyr, a metallicity Z= 0.0006 and α-enhanced chemical mixture (corresponding to an iron content of [Fe/H]=–1.84 dex, in agreement with M09). The color excess is the same quoted by Harris (1996, 2010 edition), based on the photometry by Cudworth (1986), while we derived a slightly fainter ($\sim$0.11 mag) distance modulus.

3. Iron abundance

The iron abundances have been derived by comparing observed and theoretical equivalent widths (EWs) by means of the code GALA (Mucciarelli et al. 2013a). EWs have been measured with the code DAOSPEC (Stetson & Pancino 2008) run through the wrapper 4DAO (Mucciarelli 2013) that allows a visual inspection of the best-fit Gaussian profile for each individual line. Model atmospheres have been computed with the code ATLAS9[2] assuming 1-dimensional, plane-parallel geometry, no overshooting in the computation of the convective flux and adopting the new opacity distribution functions by Castelli & Kurucz (2004) computed with an enhanced chemical composition for the α-elements (while for all the other elements a solar [X/Fe] abundance ratio is assumed). The metallicity [M/H] of the model atmosphere for each star has been chosen according to the average [Fe/H] derived from FeII lines, being most of the iron in the ionized stage in the atmosphere of late-type stars.

First guess parameters for effective temperature (T_{eff}) and surface gravities (log g) have been calculated from the photometry. T_{eff} has been derived from the color-T_{eff} transformations by Alonso et al. (1999), by averaging the values obtained from different de-reddened broad-band colors, namely $(U - B)_0$, $(B - V)_0$, $(V - I)_0$, $(V - K_s)_0$ and $(J - K_s)_0$. Surface gravities have been derived through the Stefan-Boltzmann relation, assuming the average T_{eff} , the bolometric corrections by Alonso et al. (1999) computed with the average T_{eff} and the stellar masses obtained from the best-fit isochrone. For most of the stars we adopted a

---

[2]http://wwwuser.oats.inaf.it/castelli/sources/atlas9codes.html

mass of 0.78 $M_\odot$ (appropriate for RGB stars, according to the best-fit theoretical isochrone). Three targets are identified as likely AGB stars, according to their positions in the optical CMDs (they are marked as empty triangles in Fig. 1). We assumed for these stars a mass of 0.65 $M_\odot$, corresponding to the median value of the mass distribution of the horizontal branch stars of M22 (obtained by using the zero age horizontal branch models of the BaSTI database). The position of two other stars (marked as empty squares in Fig. 1) could also be compatible with the AGB but the small color separation from the RGB makes it difficult to unambiguously assign these targets to a given evolutionary sequence. For these two stars we assume conservatively a mass of 0.78 $M_\odot$ and checking that the impact of a different mass on the iron abundances is very small: assuming the AGB mass, [FeII/H] changes by ~0.03 dex, while [FeI/H] does not change.

Because the targets span relatively large ranges in the parameter space ($\delta T_{\rm eff}$~700 K and $\delta \log g$~1.5 dex, according to the photometric estimates), the use of an unique linelist is inadvisable, because the line blending conditions vary with the evolutionary stage of the stars. Hence, a suitable linelist has been defined for each individual target, by using a specific synthetic spectrum calculated with the code SYNTHE (see Sbordone et al. 2004, for details), adopting the photometric parameters and including only transitions predicted to be unblended and detectable in the observed spectrum. Each linelist has been refined iteratively: after a first analysis, the selected transitions have been checked with synthetic spectra calculated with the new parameters and including the precise chemical composition obtained from the analysis. The oscillator strengths for FeI lines are from the compilation by Fuhr, Martin & Wiese (1988) and Fuhr & Wiese (2006), while for FeII lines we adopted the recent atomic data by Melendez & Barbuy (2009). Concerning the van der Waals damping constants, the values calculated by Barklem, Piskunov & O'Mara (2000) are adopted whenever possible, while for other transitions they were computed according to the prescriptions of Castelli (2005). The reference solar value is 7.50 (Grevesse & Sauval 1998). EW, excitation potential and oscillator strength are listed in Table 1. The iron abundances have been derived from 130-200 FeI lines and 15-20 FeII lines, leading to internal uncertainties arising from the EW measurements (estimated as the line-to-line scatter divided to the square root of the number of used lines) of the order of 0.01 dex (or less) for FeI and 0.01-0.02 dex for FeII. The chemical analysis has been performed with three different approaches to constrain $T_{\rm eff}$ and $\log g$, while the microturbulent velocities ($v_{\rm turb}$) have been constrained by imposing no trend between the iron abundance and the line strength, expressed as $\log(EW/\lambda)$. The total uncertainty in the chemical abundance has been computed by summing in quadrature the internal uncertainty and that arising from the atmospheric parameters, the latter being estimated according to the different method adopted (as discussed below). Table 2 summarises the average [FeI/H] and [FeII/H] abundances obtained with the different methods.

3.1. Method (1): spectroscopic T_{eff} and log g

The values of T_{eff} have been derived by erasing any trend between the iron abundance obtained from FeI lines and the excitation potential (χ), while log g have been derived by requiring the same abundance from FeI and FeII lines. Because of the large number of FeI lines, well distributed over a wide range of χ values, the spectroscopic T_{eff} are constrained with internal uncertainties of about 30-50 K, while the internal uncertainties on log g are $\sim$0.03-0.05. Uncertainties in v_{turb} are of about 0.1 km/s (this value is valid also for the other methods where the same approach is used to derive v_{turb}). We assumed a typical uncertainty of $\pm$0.05 dex in the metallicity [M/H] of the model atmosphere; this has a negligible impact on [FeI/H] but leads to variations of $\pm$0.02-0.04 dex in [FeII/H].

The [Fe/H] distributions thus derived from neutral and single ionized lines are shown in the left panel of Fig. 2, as generalized histograms. The two distributions are, by construction, very similar to each other (because of the adopted constraint to derive log g) and $\sim$0.5 dex wide, with an average value of [Fe/H]=–1.92$\pm$0.03 (σ=0.13 dex) for both [FeI/H] and [FeII/H]. In order to evaluate whether the observed scatter is compatible with an intrinsic spread, we adopted the maximum likelihood (ML) algorithm described in Mucciarelli et al. (2012), which provides the intrinsic scatter (σ_{int}) of the metallicity distributions by taking into account the uncertainties of each individual star. Both the iron distributions have a non-zero scatter, with σ_{int}=0.13$\pm$0.02 dex. This result is qualitatively similar to that of M09, who obtained a broad Fe distribution adopting the same approach to derive the atmospheric parameters.

3.2. Method (2): spectroscopic T_{eff} and photometric log g

The values of T_{eff} have been constrained spectroscopically, as done in the method (1), while those of log g have been derived through the Stefan-Boltzmann relation. In the computation of log g, we adopted the distance modulus, stellar masses, color excess and bolometric corrections used for the guess parameters, together with the spectroscopic T_{eff}. The internal uncertainty of the photometric log g has been computed including the uncertainties in the adopted T_{eff}, stellar mass, magnitudes and differential reddening corrections, leading to a total uncertainty of about 0.05 dex. Errors in distance modulus and color excess have been neglected because they impact systematically all the stars, while we are interested in the star-to-star uncertainties only. This approach allows to benefit at best from all the spectroscopic and photometric pieces of information in hand, minimizing the impact (mainly on T_{eff}) of the uncertainties in the differential and absolute reddening. The atmospheric parameters and the [FeI/H] and [FeII/H] abundance ratios derived with this method are listed

in Table 3.

By adopting this method, which (at odds with the previous one) does not impose ionization balance, we find that, for most of the targets, a large difference between [FeI/H] and [FeII/H]. The [FeI/H] and [FeII/H] distributions are shown in the right panel of Fig. 2. At variance with the previous case, the two distributions look very different: the distribution of [FeI/H] spans a range of ∼0.5 dex, with an average value of –1.92±0.04 (σ=0.16 dex), while the [FeII/H] distribution is narrow and symmetric, with an average value of –1.75±0.01 dex (σ= 0.04 dex). The ML algorithm provides an intrinsic spread σ_{int}=0.15±0.02 dex for the [FeI/H] distribution, while the [FeII/H] distribution is compatible with a negligible intrinsic scatter (σ_{int}= 0.00±0.02 dex).

To illustrate this difference between [FeI/H] and [FeII/H], Fig. 3 shows some FeI and FeII lines in the spectra of stars #200080 (where [FeI/H] is 0.29 dex lower than [FeII/H]) and #88 (where [FeI/H] and [FeII/H] differ by 0.05 dex only). In the first case, the synthetic spectrum calculated with the average abundance derived from FeII lines (red solid line) is not able to reproduce the FeI lines. The latter are always weaker than those of the synthetic spectrum, regardless of their χ and line strength, thus suggesting that the discrepancy is not due to inaccuracies in T_{eff} and/or v_{turb} (otherwise a better agreement would have been found for high-χ lines, less sensitive to T_{eff}, and/or for weak lines, less sensitive to v_{turb}). On the other hand, the synthetic spectrum computed with the [FeI/H] abundance (blue dashed line) does not fit the FeII line, that is stronger than that predicted by the synthetic spectrum. In the case of star #88 the situation is different and an unique Fe abundance is able to well reproduce both FeI and FeII lines.

3.3. Method (3): photometric T_{eff} and log g

As an additional check, the analysis has been performed keeping T_{eff} and log g fixed at the guess values derived from the photometry (see Section 3), and optimizing spectroscopically only v_{turb}. This set of parameters is very similar to that obtained with method (2), with the average differences, in the sense of method (3) - method (2), of +58±12 K (σ= 50 K) in T_{eff}, +0.02±0.005 (σ=0.02) in log g and +0.04±0.02 kms^{-1} (σ= 0.08 kms^{-1}) in v_{turb}. In particular, we note that spectroscopic and photometric T_{eff} agree very well, and their differences do not show trends with the photometric T_{eff}, as visible in Fig. 5 where the difference between T_{eff} from method (3) and (2) are shown as a function of the spectroscopic T_{eff}.

Fig. 4 shows the Fe abundance distributions obtained with the average photometric

parameters (upper-left panel) and using the individual broad-band colors $(U-B)_0$, $(B-V)_0$, $(V-I)_0$, $(V-K_s)_0$, $(J-K_s)_0$. In all cases, the [FeII/H] distribution is single-peaked and narrow, well consistent with that obtained from method (2). Instead, whatever color is adopted, the [FeI/H] distribution always has a much larger (by a factor of 2-3) dispersion than that obtained for [FeII/H], similar to the finding of method (2). In particular, when we consider the average photometric parameters, the ML algorithm provides intrinsic scatter of 0.12±0.02 for [FeI/H] and 0.00±0.02 for [FeII/H]. Because the results obtained with this method agree with those obtained with method (2), and the star-to-star uncertainties in spectroscopic $T_{\rm eff}$ are smaller than the photometric ones (which are also affected by the uncertainties on the differential reddening corrections), in the following we refer only to method (2) as alternative approach to method (1).

4. A sanity check: NGC 6752

As a sanity check, UVES-FLAMES archival spectra of 14 RGB stars in the GC NGC 6752 observed with the Red Arm 580 grating have been analysed following the same procedure used for M22. NGC 6752 is a well-studied GC that can be considered as a standard example of *genuine* GC, with no intrinsic iron spread (see e.g. Yong et al. 2005; Carretta et al. 2009a)[3] and with a metallicity comparable with that of M22. This approach allows to remove any systematics due to the adopted atomic data, solar reference values, model atmospheres, method to measure EWs and to derive the atmospheric parameters. When the parameters are derived following method (2), we derive average abundances [FeI/H]=–1.62±0.01 dex ($\sigma=0.04$ dex) and [FeII/H]=–1.58±0.01 dex ($\sigma=0.04$ dex), in good agreement with the previous estimates available in the literature. In this case, the two iron distributions (shown in Fig. 6) have small observed dispersions, both compatible with a negligible scatter within the uncertainties, as demonstrated by the ML algorithm. The two distributions are compatible with each other also in terms of their shape, at variance with those of M22. The same results are obtained when the parameters are all derived spectroscopically. This test demonstrates that: (i) the different [FeI/H] and [FeII/H] distributions obtained for M22 with methods (2) and (3) are not due to the adopted procedure; (ii) in a normal GC the shape of [FeI/H] and [FeII/H] distributions are not significantly different.

---

[3] Yong et al. (2013) performed a strictly differential line-by-line analysis on 37 RGB stars of NGC 6752 by using high-quality UVES spectra, finding an observed spread in [Fe/H], 0.02 dex, larger of a factor of 2 than the internal uncertainties. This small intrinsic spread could reflect He variations and/or real inhomogeneities in the cluster iron content. Because such chemical inhomogeneities can be revealed only when the internal uncertainties are smaller than ∼0.02 dex, for our purposes we can consider NGC 6752 as a *genuine* GC.

5.   No iron spread in M22

The new analysis of the sample of giant stars already discussed in M09 leads to an unexpected result: an iron abundance spread in M22 is found when FeI lines are used, independently of the adopted spectroscopic or photometric gravities. *This scatter totally vanishes when the iron abundance is derived from FeII lines and photometric gravities are used.* In the case of spectroscopic gravities, the abundances from FeII lines are forced to match those from FeI lines, thus producing a broad [FeII/H] distribution. Given that the adoption of photometric gravities leads to a broad [FeI/H] distribution and a narrow, mono-metallic [FeII/H] distribution, which one should we trust? In principle, FeII lines are most trustworthy than FeI lines to determine the iron abundance, because FeII is a dominant species in the atmospheres of late-type stars (where iron is almost completely ionized) and its lines are unaffected by NLTE effects, at variance with the FeI lines (see e.g. Kraft & Ivans 2003; Mashonkina et al. 2011).

The analysis of the results shown in Fig. 2 and 4 suggests that the adoption of method (1) tends to produce an artificial spread of [FeII/H] toward low metallicities. Since [FeII/H] strongly depends on the adopted values of logg, this implies that gravities are severly under-estimated in method (1). This bias is clearly revealed when the stellar masses corresponding to the spectroscopic values of log g values are computed. We estimated the stellar masses by inverting the Stefan-Boltzmann equation and assuming the spectroscopic log g derived with method (1). The derived masses range from 0.12 to 0.79 $M_\odot$, with a mean value of 0.46 $M_\odot$ and a dispersion of 0.2 $M_\odot$. Note that $\sim$70% of the stars have masses below 0.6 $M_\odot$. Such low values, as well as the large dispersion of the mass distribution, are unlikely for a sample dominated by RGB stars, with expected masses close to 0.75-0.80 $M_\odot$. In particular, 10 target stars have log g that would require masses below 0.5 $M_\odot$, thus smaller than the typical mass of the He-core of GC giant stars at the luminosity level of our targets. Such very low masses cannot be justified even in light of the uncertainties in the mass loss rate (Origlia et al. 2014). A similarly wide mass distribution is obtained by adopting the spectroscopic parameters by M09, leading to a mass range between 0.34 and 1.19 $M_\odot$. In that case, three stars have masses larger than 0.8 $M_\odot$, corresponding to the typical mass of a turnoff star of M22. For comparison, the masses derived from the spectroscopic log g of the spectral sample of NGC 6752 (see Section 4) cover a small and well reasonable range, from 0.65 to 0.85 $M_\odot$, with an average value of 0.75 $M_\odot$ (σ=0.06 $M_\odot$).

Fig. 7 shows the behavior of the difference [FeI/H]-[FeII/H], as derived with method (2), as a function of the stellar masses, as derived from the spectroscopic gravities in method (1). The mass intervals expected for RGB and AGB stars in the luminosity range of our spectroscopic targets are shown as grey shaded regions. A clear trend between the [FeI/H]-

[FeII/H] difference and the stellar mass is found. The stars with the largest difference between FeI and FeII abundances are also those where the spectroscopic log g requires an unrealistically low mass, while for the stars where [FeI/H] is consistent with [FeII/H] the spectroscopic log g provide masses in reasonable agreement with the theoretical expectations. This demonstrates that the spectroscopic gravities needed to force [FeII/H] matching the low-abundance tail of the [FeI/H] distribution lead to unreliable stellar masses. Since this is the only case in which [Fe II/H] shows significant spread, we have to conclude that the observed large iron distribution is not real. The correct diagnostic of iron content therefore are the Fe II lines analyzed under the assumption of photometric gravities. These always lead to a narrow iron distribution (see Figs. 2 and 4), thus implying that no iron spread is observed in M22.

An additional confirmation of the different behavior of neutral and ionized lines in our sample is provided by the analysis of the titanium transitions, because this element is one of the few species that provides a large number of both neutral and single ionized lines. The oscillator strengths are from Martin, Fuhr & Wiese (1988) and Lawler et al. (2013) for Ti I lines and from Wood et al. (2013) for Ti II lines. The [TiI/H] and [TiII/H] abundances exhibit the same behavior discussed above for the Fe abundances. When the spectroscopic gravities are used, both the distributions are broad, with an observed scatter of ∼0.2 dex (see left panel of Fig. 8). On the other hand, when the photometric gravities are adopted (see Table 3), the [TiII/H] distribution is consistent with null intrinsic scatters, while that of [TiI/H] remains broad and skewed toward low abundances (right panel of Fig. 8). We note that the difference [TiI/H]-[TiII/H] strongly correlates with the difference [FeI/H]-[FeII/H], with a Spearman rank correlation coefficient C_S=+0.956 that provides a probability of ∼ 10^{-8} that the two quantities are not correlated. Hence, the analysis of [TiI/H] and [TiII/H] reinforces the scenario where the abundances from neutral lines in most of the M22 stars are biased, providing distributions (artificially) larger than those from single ionized lines.

6. The s-process elements abundance

M09 and Marino et al. (2011b) found that M22 has, together with a dispersion in the iron content, an intrinsic spread in the abundances of s-process elements. In light of the results described above, we derived abundances also for these elements, by adopting the parameters obtained with method (2) and measuring Y II, Ba II, La II and Nd II lines. For Y and Nd the abundances have been obtained with GALA from the EW measurement, as done for the Fe and Ti lines, and adopting the oscillator strengths available in the Kurucz/Castelli

linelist. Ba II and La II lines are affected by hyperfine and isotopic splittings. The linelists for the La II lines are from Lawler et al. (2001), while those for the Ba II lines from the NIST database [4]. Only for these two elements, the abundances have been derived with our own code SALVADOR (A. Mucciarelli et al. in preparation) that performs a χ^2-minimization between observed and synthetic spectra calculated with the code SYNTHE.

For all these elements, we found that the absolute abundances show large star-to-star variations, with observed scatters between ∼0.2 and ∼0.3 dex, depending on the element. These spreads are not compatible within the uncertainties. Because of the possible occurrence of the NLTE effects, the abundance ratios [X/Fe] (see Table 4) have been estimated by using the FeII abundances as reference; in fact, for these elements the chemical abundances have been derived only from single ionized transitions, which are less sensitive to the overionization (or sensitive to it in a comparable way to the FeII lines; see e.g. the discussion in Ivans et al. 2001). The [X/FeII] abundance ratios show significant intrinsic spreads, as confirmed by the ML algorithm. Note that, if we adopt FeI abundances as reference, the [X/FeI] abundance ratios still display an intrinsic scatter, because the observed spread in the absolute abundances for these s-process elements is larger than that measured from the FeI lines.

Fig. 9 shows the behavior of each s-process element abundance ratio as a function of the difference between [FeI/H] and [FeII/H]. In all the cases, a clear trend between [X/FeII] and [FeI/H]-[FeII/H] is detected, in the sense that the stars characterized by higher s-process abundances display a better agreement between FeI and FeII. In the case of Y, Ba and Nd, we find two distinct and well separated groups of stars, while for La the behavior is continuous, with no clear gap. Finally, Fig. 10 plots the behavior of <[s/FeII]>, obtained by averaging together the four abundance ratios, as a function of [FeI/H]-[FeII/H], confirming the existence of two groups of stars, with different [s/Fe] and [FeI/H] (but the same [FeII/H]). This finding resembles the results by M09 who identify two groups of stars, named *s-poor* and *s-rich*.

7. Discussion: re-thinking M22

The main results and conclusions of this work are summarized as follows:

- The new analysis of M22 presented here demonstrates that this GC is mono-metallic and that the previous claim of a metallicity scatter was due to a systematic under-

---

[4]http://physics.nist.gov/PhysRefData/ASD/lines_form.html

estimate of the FeI abundance combined with the use of spectroscopic gravities. When photometric log g are adopted, the FeII lines provide the same abundance for all the stars, regardless of the adopted method to estimate T_{eff}.

- In light of this result, the formation/evolution scenario for M22 must be deeply re-thought. The homogeneity in its iron content suggests that M22 was not able to retain the SN ejecta in its gravitational well. Hence, it is not necessary to invoke that the cluster was significantly more massive at its birth and that it subsequently lost a large amount of its mass. The observed unimodal [FeII/H] distribution rules out the possibility that M22 is the remnant of a now disrupted dwarf galaxy, because these systems are characterized by a wide range of metallicity, due to the prolonged star-formation activity (see Tolstoy, Hill & Tosi 2009, and references therein). Also, comparisons between M22 and ω Centauri (Da Costa & Marino 2011) are undermined by the homogeneity in the [FeII/H] abundance of M22. On the other hand, M22 cannot be considered as a *genuine* GC, because of the intrinsic spread in heavy s-process elements abundances, pointing out the occurence of a peculiar chemical enrichment (probably from AGB stars) in this cluster, at variance with most of the GCs where s-process elements do not show intrinsic scatters (D'Orazi et al. 2010).

- M09 and Marino et al. (2011b) discussed the possibility that M22 is the product of a merging between two GCs with different chemical composition. In light of our new analysis, this scenario appears unlikely, even if it cannot be totally ruled out. In this framework, M22 should form from the merging between two clusters with the same Fe content, but characterized by different s-process element abundances. While clusters with comparable metallicity and different s-process abundance are indeed observed (for instance M4 and M5; Ivans et al. 1999, 2001), in this scenario the cluster with normal s-process abundances should be composed mainly by stars with a large difference between [FeI/H] and [FeII/H], while the second cluster should have stars with enhanced s-process abundances and similar [FeI/H] and [FeII/H] (see Fig. 10).

- As a possible working hypothesis to explain the observed behavior of [FeI/H] and [FeII/H], we note that the difference between [FeI/H] and [FeII/H] is qualitatively compatible with the occurrence of NLTE effects driven by overionization. These effects are known to affect mainly the less abundant species, like FeI, and to have a negligible/null impact on the dominant species, like FeII (see e.g. Thévenin & Idiart 1999; Mashonkina et al. 2011; Fabrizio et al. 2012). Under NLTE conditions, the spectral lines of neutral ions are weaker than in LTE. Hence, when the line formation is calculated in LTE conditions (as done in standard analyses), the resulting abundance of neutral lines will be correspondingly lower.

The same interpretative scheme can be applied to M22. A large and intrinsically broad Fe distribution is obtained only from FeI lines, according to the systematic underestimate of the Fe abundance obtained when lines affected by overionization are analysed in LTE. On the other hand, FeII lines are not affected by NLTE and they provide (when photometric log g are used) the correct abundance, leading to a narrow abundance distribution.

- The mismatch between [FeI/H] and [FeII/H] observed in M22 resembles those found in the GCs M5 (Ivans et al. 2001), 47 Tucanae (Lapenna et al. 2014) and NGC 3201 (Mucciarelli et al. 2015). In these cases, the different behavior observed for FeI and FeII lines is restricted to AGB stars only, where FeI lines provide abundances systematically lower than those from FeII lines, while RGB stars have similar [FeI/H] and [FeII/H]. However, the situation is more complex in M22, because a large difference between [FeI/H] and [FeII/H] is observed in most of the stars and not only in AGB stars. Among the target stars of M22, three are identified as AGB stars, according to their positions in the CMDs. Two of them have a large Fe difference, [FeI/H]-[FeII/H]=– 0.29 and –0.44 dex, while for the third star FeI and FeII lines provide almost the same abundance. The other two possible AGB stars (empty squares in Fig. 1) have Fe differences of –0.21 dex. On the other hand, comparable differences are observed among some RGB stars. For instance, the two faintest stars of the sample (#221 and #224) are clearly RGB stars (see Fig. 1 and 7), because they are located at the luminosity level where the color separation between RGB and AGB is the largest. On the other hand, these two stars (with very similar atmospheric parameters and [FeII/H]) have different [FeI/H] abundances: star #224 has a difference of [FeI/H]-[FeII/H]=–0.14 dex, while star #221 has [FeI/H]-[FeII/H]=–0.29 dex. If departures from LTE are the reasons for the observed discrepancy between [FeI/H] and [FeII/H] (and between [TiI/H] and [TiII/H]), this finding challenges the available NLTE calculations (see e.g. Lind et al. 2012; Bergemann et al. 2012), in which stars with very similar parameters are expected to have the same NLTE corrections. New NLTE calculations should be performed to investigate this hypothesis, with the constraint to reproduce simultaneously the discrepancies in Fe and Ti.

- We found that the difference between [FeI/H] and [FeII/H] is correlated with the s-process element abundances. The behavior is quite puzzling, because the stars with an anomalous difference between [FeI/H] and [FeII/H] are those with *normal* s-process abundances, compatible with the abundances observed in most of the GCs and in the Galactic field stars of similar metallicity (see e.g. Fig.3 in Venn et al. 2004). On the other hand, the stars enriched in s-process elements show a good agreement between [FeI/H] and [FeII/H]. *Whatever the mechanism responsible to spread [FeI/H] is, it must*

be also responsible for the peculiar behavior of the s-process element abundances.

- We confirm the claim already suggested by Lapenna et al. (2014) and Mucciarelli et al. (2015): chemical analyses based on FeI lines and spectroscopic gravities can lead to spurious abundance spreads. In light of these results, any claim of intrinsic iron spread in GCs should be always confirmed with an analysis based on FeII lines and photometric gravities. If the abundance spread is real, it should be detected also when FeII lines and photometric log g are adopted, since FeII lines are the most reliable indicators of the iron abundance. All the GCs with anomalous intrinsic Fe spreads observed so far (see Marino et al. 2015, for an updated list) deserve new analyses in light of this effect, in order to firmly establish whether these spreads are real or spurious.

REFERENCES

Alonso, A., Arribas, S., & Martínez-Roger, C. 1999, A&AS, 140, 261

Barklem, P. S., Piskunov, N., & O'Mara, B. J., 2000, A&AS, 142, 467

Bastian, N., Lamers, H. J. G. L. M., de Mink, S. E., Longmore, S. E., Goodwin, S. P., & Gieles, M., 2013, MNRAS, 436, 2398

Bergemann, M., Lind, K., Collet, R., Magic, Z., & Asplund, M., 2012, MNRAS, 427, 27

Cardelli, J. A., Clayton, G. C., & Mathis, J. S., 1989, ApJ, 345, 245

Carretta, E., Bragaglia, A., Gratton, R., D'Orazi, V., & Lucatello, S., 2009a, A&A, 508, 695

Carretta, E., Bragaglia, A., Gratton, R., & Lucatello, S., 2009b, A&A, 505, 139

Carretta, E., Bragaglia, A., Gratton, R. G., Lucatello, S., Bellazzini, M., Catanzaro, G., Leone, F. , Momany, Y., Piotto, G., & D'Orazi, V., 2010, ApJ, 714L, 7

Carretta, E., Gratton, R. G., Lucatello, S., Bragaglia, A., Catanzaro, G., Leone, F., Momany, Y., D'Orazi, V., Cassisi, S., D'Antona, F., & Ortolani S., 2010, ApJ, 722L, 1

Castelli, F., 2005, Mem. Soc. Astron. Ital. Suppl., 8, 44

Castelli, F., & Kurucz, R. L., 2004, arXiv:astro-ph/0405087

Cohen, J. G., 1981, ApJ, 247, 869

Cohen, J. G., Kirby, E. N., Simon, J. D., & Geha, M., 2010, ApJ, 725, 288

Cohen, J. G., & Kirby, E. N. 2012, ApJ, 760, 86

Cudworth K.M., 1986, AJ 92, 348

Da Costa, G. S. & Marino, A. F., 2011, PASA, 28, 28

Dekker, H. et al., 2000, SPIE, 4008, 534

Decressin, T., Meynet, G., Charbonell, C., Prantzos, N., & Ekstrom, S., 2007, A&A, 464, 1029

De Mink, S. E., Pols, O. R., Langer, N., & Izzard, R. G., 2009, A&A, 507L, 1

Denissenkov, P. A. & Hartwick, F. D. A., 2014, MNRAS, 437L, 21

D'Ercole, A., Vesperini, E., D'Antona, F., McMillan, S. L. W., & Recchi, S., 2008, MNRAS, 391, 825

D'Orazi, V., Gratton, R., Lucatello, S., Carretta, E., Bragaglia, A., & Marino, A. F., 2010, ApJ, 719L, 213

Fabrizio, M. et al., 2012, PASP, 124, 519

Ferraro, F. R., Dalessandro, E., Mucciarelli, A., Beccari, G., Rich, R. M., Origlia, L., Lanzoni, B., Rood, R. T., Valenti, E., Bellazzini, M., Ransom, S. M., & Cocozza, G., 2009, Nature, 462, 483

Fuhr, J. R., Martin, G. A., & Wiese, W. L., 1988, JPCRD, 17S

Fuhr, J. R., & Wiese, W. L., 2006, JPCRD, 35, 1669

Gratton, R. G., 1982, A&A, 115, 171

Grevesse, N., & Sauval, A. J., 1998, SSRv, 85, 161

Harris, W. E., 1996, Astronomical Journal, 112, 1487

Johnson, C. I., & Pilachowski, C. A., 2010, ApJ, 722, 1373

Kirby, E. N., Guhathakurta, P., Bolte, M., Sneden, C., & Geha, M. C., 2009, ApJ, 705, 328

Kraft, R. P. & Ivans, I. I., 2003, PASP, 115, 143

Kunder, A., et al., 2013, AJ, 146, 119

Ibata, R., Sollima, A., Nipoti, C., Bellazzini, M., Chapman, S. C., & Dalessandro, E., 2011, ApJ, 738, 286

Ivans,I. I., Sneden, C., Kraft, R. P., et al. 1999, AJ, 118, 1273

Ivans, I. I., Kraft, R. P., Sneden, C., et al. 2001, AJ, 122, 1438

Lardo, C., Milone, A. P., Marino, A. F., Mucciarelli, A., Pancino, E., Zoccali, M., Rejkuba, M., Carrera, R. & Gonzalez, O., 2012, A&A, 541, 141

Larsen, S. S., Brodie, J. P., Grundahl, F., & Strader, J., 2014, ApJ, 797, 15

Lapenna, E., Mucciarelli, A., Lanzoni, B., Ferraro, F. R., Dalessandro, E., Origlia, L., & Massari, D., 2014,ApJ, 797, 124

Lawler, J.E., Bonvallet, G., & Sneden, C., 2001, ApJ, 556, 452

Lawler, J. E., Guzman, A., Wood, M. P., Sneden, C. & Cowan, J. J., 2013, ApJS, 205, 11

Lind, K., Bergemann, M., & Asplund, M. 2012, MNRAS, 427, 50

Marino, A. F., Milone, A. P., Piotto, G., Villanova, S., Bedin, L. R., Bellini, A., & Renzini, A., 2009, A&A, 505, 1099

Marino, A. F. et al., 2011, ApJ, 731, 64

Marino, A. F. et al., 2011, A&A, 532, 8

Marino, A. F. et al., 2012, A&A, 541, 15

Marino, A. F. et al., 2015, MNRAS, 450, 815

Martin, G. A., Fuhr, J. R., & Wiese, W. L., 1988, JPCRD, 17S

Mashonkina, L., Gehren, T., Shi, J.-R., Korn, A. J., & Grupp, F., 2011, A&A, 528, 87

Massari, D., Mucciarelli, A., Ferraro, F. R., Origlia, L., Rich, R. M., Lanzoni, B., Dalessandro, E., Valenti, E., Ibata, R., Lovisi, L., Bellazzini, M., & Reitzel, D., 2014, ApJ, 795, 22

Milone, A. P. et al., 2012, A&A, 540, 16

Melendez, J., & Barbuy, B., 2009, A&A, 497, 611

Monaco, L., Pancino, E., Ferraro, F. R., & Bellazzini, M., 2004, MNRAS, 349, 1278

Mucciarelli, A., Origlia, L., Ferraro, F. R., & Pancino, E., 2009, ApJ, 695L, 134

Mucciarelli, A., Bellazzini, M., Ibata, R., Merle, T., Chapman, S. C., Dalessandro, E., & Sollima, A., 2012, MNRAS, 426, 2889

Mucciarelli, A., Pancino, E., Lovisi, L., Ferraro, F. R., & Lapenna, E. 2013, ApJ, 766, 78

Mucciarelli, A., 2013, arXiv1311.1403

Mucciarelli, A., Lapenna, E., Massari, D., Ferraro, F. R. & Lanzoni, B., 2015, ApJ, 801, 69

Origlia, L., Ferraro, F. R., Bellazzini, M., & Pancino, E., 2003, ApJ, 591, 916

Origlia, L., Rich, R. M., Ferraro, F. R., Lanzoni, B., Bellazzini, M., Dalessandro, E., Mucciarelli, A., Valenti, E., & Beccari, G., 2011, ApJ, 726L, 20

Origlia, L., Massari, D., Rich, R. M., Mucciarelli, A., Ferraro, F. R., Dalessandro, E., & Lanzoni, B., 2013, ApJ, 779L, 5

Origlia, L., Ferraro, F. R., Fabbri, S., Fusi Pecci, F., Dalessandro, E., Rich, R. M., & Valenti, E. 2014, A&A, 564, A136

Pancino, E., Mucciarelli, A., Sbordone, L., Bellazzini, M., Pasquini, L., Monaco, L. & Ferraro, F. R., 2011, A&A, 527, 18

Pasquini, L., et al., 2000, SPIE, 4008, 129

Pietrinferni, A., Cassisi, S., Salaris, M. & Castelli, F., 2006, ApJ, 642, 797

Pilachowski, C., Leep, E. M, Wallerstein, G., & Peterson, R. C., 1982, ApJ, 263, 187

Sbordone, L., Bonifacio, P., Castelli, F., & Kurucz, R. l., 2004, MSAIS, 5, 93

Skrutskie, M. F. et al. 2006, AJ, 131, 1163

Simmerer, J., Ivans, I. I., Filler, D., Francois, P., Charbonnel, C., Monier, R., & James, G., 2013, ApJ, 764L, 7

Stetson, P. B., & Pancino, E., PASP, 120, 1332 K. 2005, PASJ, 57, 27

Thévenin, F., & Idiart, T. P. 1999, ApJ, 521, 753

Tolstoy, E., Hill, V., & Tosi, M., 2009, ARA&A, 47, 371

Venn, K. A., Irwin, M., Shetrone, M. D., Tout, C. A., Hill, V., & E. Tolstoy, 2004, AJ, 128, 1177

Willman, B. & Strader, J., 2012, AJ, 144, 76

Wood, M. P., Lawler, J. E., Sneden, C., & Cowan, J. J., 2013, ApJS, 208, 27

Yong, D., Grundahl, F., Nissen, P. E., Jensen, H. R., & Lambert, D. L., 2005, A&A, 438, 875

Yong, D., Melendez, J., Grundahl, F., Roederer, I. U., Norris, J. E., Milone, A. P., Marino, A. F., Coelho, P., McArthur, B. E., Lind K., Collet, R., & Asplund, M., 2013, MNRAS, 434, 3542

Yong, D., Roederer, I. U., Grundahl, F., Da Costa, G. S., Karakas, A. I., Norris, J. E., Aoki, W., Fishlock, C. K., Marino, A. F., Milone, A. P., & Shingles, L. J., 2014, MNRAS, 441, 3396

Yong, D., Grundahl, F., & Norris, J. E., 2015, MNRAS, 446, 3319

Table 1.   Star identification number, wavelength, ion, excitation potential, oscillator
strength and measured EWs for all the used transitions.

Star	λ (Å)	Ion	χ (eV)	log gf	EW (mÅ)
51	4805.415	TiI	2.340	0.070	30.4
51	4870.126	TiI	2.250	0.440	46.7
51	4885.079	TiI	1.890	0.410	76.1
51	4909.098	TiI	0.830	-2.370	15.8
51	4913.614	TiI	1.870	0.220	64.0
51	4915.229	TiI	1.890	-0.910	11.8
51	4919.860	TiI	2.160	-0.120	30.1
51	4926.148	TiI	0.820	-2.090	20.9
51	4937.726	TiI	0.810	-2.080	27.2
51	4997.096	TiI	0.000	-2.070	90.7
51	5009.645	TiI	0.020	-2.200	83.1
51	5016.161	TiI	0.850	-0.480	107.5
51	5020.026	TiI	0.840	-0.330	117.0
51	5036.464	TiI	1.440	0.140	98.9
51	5038.397	TiI	1.430	0.020	95.9
51	5043.584	TiI	0.840	-1.590	46.6
51	5045.415	TiI	0.850	-1.840	29.7
51	5052.870	TiI	2.170	-0.270	23.0
51	5062.103	TiI	2.160	-0.390	15.6
51	5065.985	TiI	1.440	-0.970	38.1

Note. — This table is available in its entirety
in machine-readable form.

Table 2. Observed and intrinsic scatters for [FeI/H] and [FeII/H] as derived from the ML algorithm and from the three methods described in the paper.

	[FeI/H]	σ_{obs}	σ_{int}	[FeII/H]	σ_{obs}	σ_{int}
Method 1	−1.92±0.03	0.14	0.13±0.02	−1.90±0.03	0.14	0.13±0.02
Method 2	−1.92±0.04	0.16	0.15±0.02	−1.75±0.01	0.04	0.00±0.02
Method 3	−1.86±0.03	0.13	0.12±0.02	−1.81±0.01	0.05	0.00±0.02

Table 3. Atmospheric parameters, [FeI/H], [FeII/H], [TiI/H] and [TiII/H] abundances for the spectroscopic targets of M22, as derived with method (1). The last line lists the average abundances with the statistical error.

Star	T_{eff} (K)	log g	v_{turb} (km/s)	[FeI/H]	[FeII/H]	[TiI/H]	[TiII/H]	Notes
51	4280	1.00	1.70	−1.70±0.02	−1.71±0.04	−1.50±0.04	−1.34±0.04	
61	4430	0.95	1.70	−1.85±0.05	−1.84±0.04	−1.74±0.06	−1.61±0.04	
71	4405	0.97	1.50	−1.90±0.04	−1.89±0.04	−1.77±0.04	−1.59±0.04	
88	4450	1.20	1.50	−1.78±0.05	−1.74±0.05	−1.67±0.08	−1.46±0.04	
221	4570	1.13	1.40	−2.04±0.04	−2.04±0.04	−2.00±0.04	−1.86±0.04	
224	4670	1.75	1.40	−1.87±0.04	−1.78±0.04	−1.76±0.05	−1.47±0.04	
200005	3920	0.00	2.20	−2.10±0.02	−1.92±0.06	−1.97±0.05	−1.74±0.05	
200006	3910	0.04	2.10	−1.84±0.03	−1.78±0.05	−1.69±0.05	−1.55±0.04	
200025	4060	0.57	1.90	−1.72±0.02	−1.75±0.05	−1.48±0.05	−1.45±0.04	
200031	4290	0.72	1.80	−1.96±0.03	−1.97±0.04	−1.85±0.05	−1.64±0.04	AGB?
200043	4300	0.73	1.70	−1.94±0.04	−1.95±0.04	−1.86±0.04	−1.69±0.05	AGB?
200068	4400	0.82	1.60	−2.00±0.04	−2.00±0.04	−1.93±0.05	−1.74±0.04	
200076	4390	0.80	1.60	−2.05±0.04	−2.06±0.04	−2.01±0.05	−1.82±0.04	
200080	4520	0.70	1.70	−2.01±0.04	−2.00±0.03	−1.96±0.05	−1.78±0.04	AGB
200083	4440	1.20	1.50	−1.73±0.04	−1.75±0.04	−1.60±0.05	−1.46±0.05	AGB
200101	4400	0.90	1.50	−1.89±0.05	−1.91±0.05	−1.77±0.05	−1.64±0.05	
200104	4490	0.59	1.70	−2.19±0.06	−2.19±0.03	−2.15±0.08	−2.00±0.03	AGB
				−1.92±0.03	−1.91±0.03	−1.81±0.04	−1.64±0.04	

Table 4.   Atmospheric parameters, [FeI/H], [FeII/H], [TiI/H] and [TiII/H] abundances for the spectroscopic targets of M22, as derived with method (2). The last line lists the average abundances with the statistical error.

Star	T_{eff} (K)	log g	v_{turb} (km/s)	[FeI/H]	[FeII/H]	[TiI/H]	[TiII/H]	Notes
51	4280	0.99	1.70	−1.70±0.02	−1.72±0.04	−1.50±0.04	−1.41±0.05	
61	4440	1.17	1.60	−1.84±0.05	−1.72±0.04	−1.76±0.06	−1.49±0.05	
71	4390	1.15	1.60	−1.94±0.03	−1.78±0.04	−1.85±0.05	−1.51±0.05	
88	4470	1.30	1.50	−1.77±0.05	−1.72±0.05	−1.66±0.08	−1.44±0.06	
221	4640	1.81	1.30	−2.00±0.05	−1.71±0.04	−1.98±0.06	−1.53±0.05	
224	4650	1.80	1.30	−1.88±0.05	−1.74±0.04	−1.79±0.07	−1.42±0.05	
200005	3900	0.30	2.20	−2.07±0.03	−1.67±0.09	−2.07±0.10	−1.62±0.06	
200006	3960	0.34	2.10	−1.80±0.04	−1.72±0.09	−1.63±0.10	−1.48±0.06	
200025	4070	0.63	1.80	−1.70±0.04	−1.71±0.07	−1.45±0.08	−1.46±0.06	
200031	4240	0.86	1.80	−2.02±0.04	−1.81±0.05	−1.98±0.07	−1.53±0.05	AGB?
200043	4270	0.93	1.70	−1.98±0.04	−1.77±0.05	−1.96±0.05	−1.56±0.06	AGB?
200068	4340	1.16	1.60	−2.10±0.05	−1.75±0.05	−2.11±0.07	−1.54±0.05	
200076	4410	1.24	1.60	−2.05±0.04	−1.82±0.04	−2.03±0.05	−1.54±0.05	
200080	4570	1.28	1.70	−2.03±0.05	−1.74±0.04	−1.99±0.06	−1.52±0.05	AGB
200083	4430	1.18	1.60	−1.76±0.04	−1.76±0.05	−1.60±0.05	−1.48±0.05	AGB
200101	4480	1.37	1.50	−1.83±0.05	−1.71±0.05	−1.71±0.06	−1.44±0.06	
200104	4520	1.36	1.70	−2.26±0.05	−1.82±0.04	−2.23±0.07	−1.55±0.05	AGB
				−1.92±0.04	−1.75±0.01	−1.84±0.05	−1.50±0.01	

Table 5.   Atmospheric parameters, [FeI/H], [FeII/H], [TiI/H] and [TiII/H] abundances for the spectroscopic targets of M22, as derived with method (3). The last line lists the average abundances with the statistical error.

Star	T_{eff} (K)	log g	v_{turb} (km/s)	[FeI/H]	[FeII/H]	[TiI/H]	[TiII/H]	Notes
51	4232	0.96	1.70	−1.76±0.05	−1.72±0.06	−1.57±0.06	−1.37±0.06	
61	4400	1.16	1.60	−1.87±0.05	−1.73±0.05	−1.81±0.06	−1.50±0.07	
71	4435	1.17	1.50	−1.88±0.05	−1.82±0.05	−1.76±0.08	−1.50±0.08	
88	4537	1.32	1.60	−1.71±0.06	−1.80±0.06	−1.53±0.06	−1.49±0.07	
221	4737	1.84	1.50	−1.90±0.05	−1.81±0.05	−1.84±0.07	−1.57±0.07	
224	4746	1.84	1.50	−1.80±0.04	−1.82±0.04	−1.65±0.07	−1.48±0.06	
200005	3992	0.34	2.20	−2.08±0.04	−1.78±0.04	−1.88±0.06	−1.62±0.07	
200006	3986	0.36	2.10	−1.80±0.05	−1.77±0.05	−1.56±0.06	−1.47±0.07	
200025	4116	0.65	1.90	−1.68±0.05	−1.81±0.05	−1.36±0.08	−1.45±0.09	
200031	4271	0.87	1.80	−1.97±0.05	−1.88±0.05	−1.93±0.06	−1.54±0.07	AGB?
200043	4351	0.97	1.70	−1.89±0.04	−1.84±0.05	−1.81±0.08	−1.58±0.08	AGB?
200068	4409	1.19	1.60	−2.00±0.05	−1.85±0.07	−1.98±0.06	−1.56±0.07	
200076	4475	1.27	1.60	−1.98±0.05	−1.87±0.05	−1.92±0.06	−1.60±0.06	
200080	4618	1.30	1.80	−1.95±0.05	−1.80±0.07	−1.90±0.06	−1.55±0.07	AGB
200083	4567	1.24	1.60	−1.61±0.05	−1.84±0.05	−1.36±0.08	−1.49±0.06	AGB
200101	4527	1.39	1.60	−1.79±0.06	−1.80±0.04	−1.62±0.06	−1.52±0.07	
200104	4655	1.41	1.70	−2.04±0.07	−1.89±0.07	−1.99±0.07	−1.63±0.09	AGB
				−1.86±0.03	−1.81±0.01	−1.73±0.05	−1.52±0.02	

Table 6.   Abundance ratios for the s-process elements Y, Ba, La and Nd.

Star	[YII/FeII]	[BaII/FeII]	[LaII/FeII]	[NdII/FeII]
51	+0.15±0.04	+0.65±0.07	+0.54±0.04	+0.48±0.04
61	−0.37±0.05	+0.04±0.08	+0.08±0.04	+0.08±0.04
71	−0.35±0.05	+0.14±0.08	+0.16±0.06	+0.07±0.04
88	+0.15±0.05	+0.66±0.08	+0.47±0.04	+0.32±0.05
221	−0.42±0.04	+0.15±0.10	+0.11±0.04	+0.00±0.05
224	+0.08±0.05	+0.51±0.07	+0.34±0.06	+0.14±0.04
200005	−0.42±0.06	+0.06±0.12	+0.03±0.05	−0.10±0.05
200006	+0.06±0.08	+0.42±0.11	+0.33±0.05	+0.33±0.05
200025	+0.09±0.05	+0.54±0.06	+0.43±0.06	+0.39±0.05
200031	−0.35±0.04	+0.03±0.08	+0.03±0.06	−0.01±0.04
200043	−0.34±0.05	+0.04±0.07	+0.04±0.04	−0.03±0.04
200068	−0.41±0.04	+0.04±0.08	+0.00±0.05	−0.05±0.04
200076	−0.37±0.04	+0.10±0.08	+0.19±0.05	−0.02±0.04
200080	−0.45±0.04	+0.13±0.09	+0.08±0.05	+0.03±0.05
200083	+0.13±0.06	+0.72±0.08	+0.58±0.04	+0.43±0.04
200101	+0.12±0.06	+0.77±0.09	+0.53±0.04	+0.37±0.05
200104	−0.45±0.04	+0.07±0.09	+0.15±0.06	−0.01±0.05
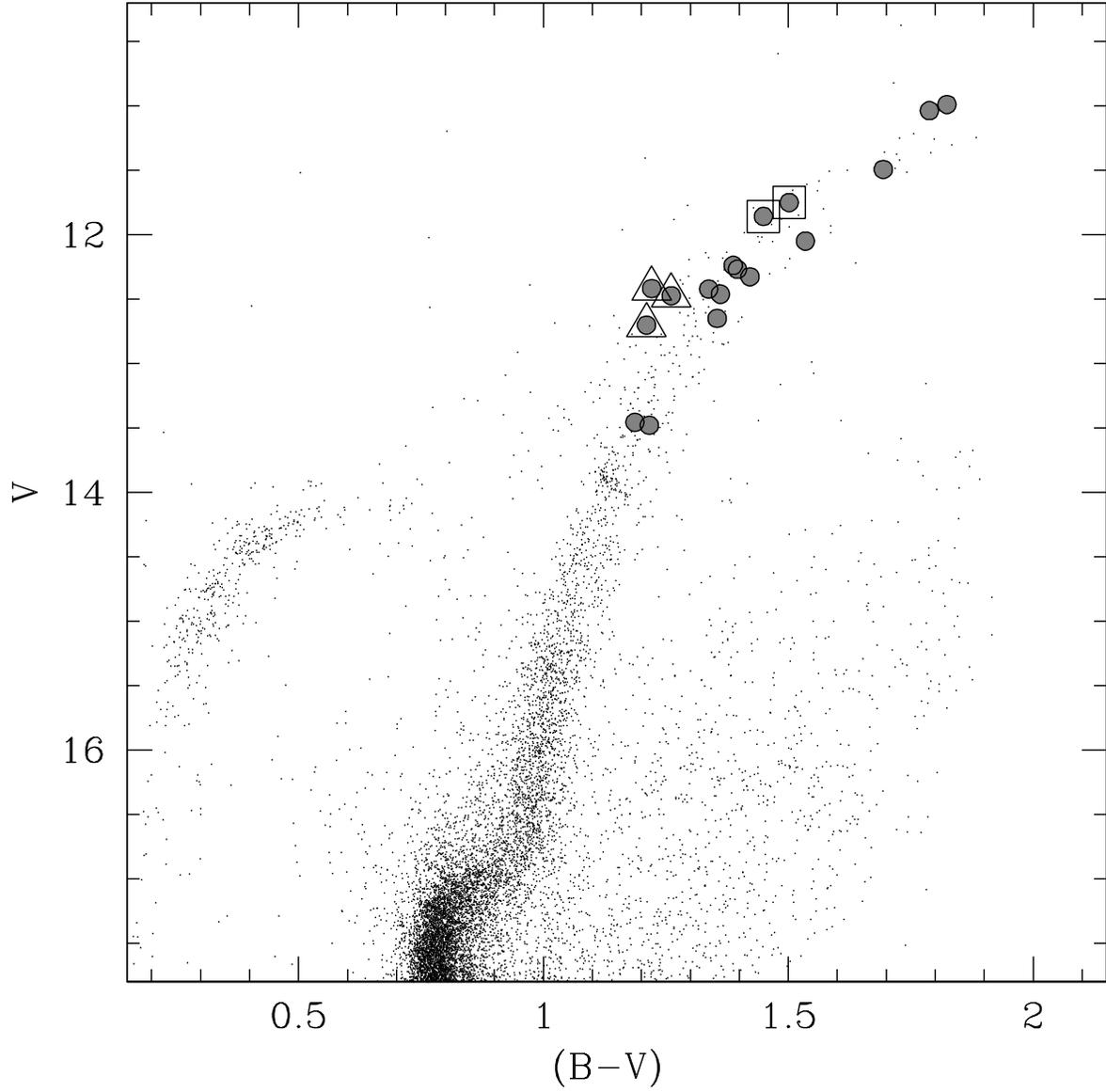
Fig. 1.— (B-V, V) color-magnitude diagram of M22 (Kunder et al. 2013) with marked as grey circles the spectroscopic targets. Empty triangles are the likely candidate AGB stars, while empty squares are possible (but not sure) AGB stars.
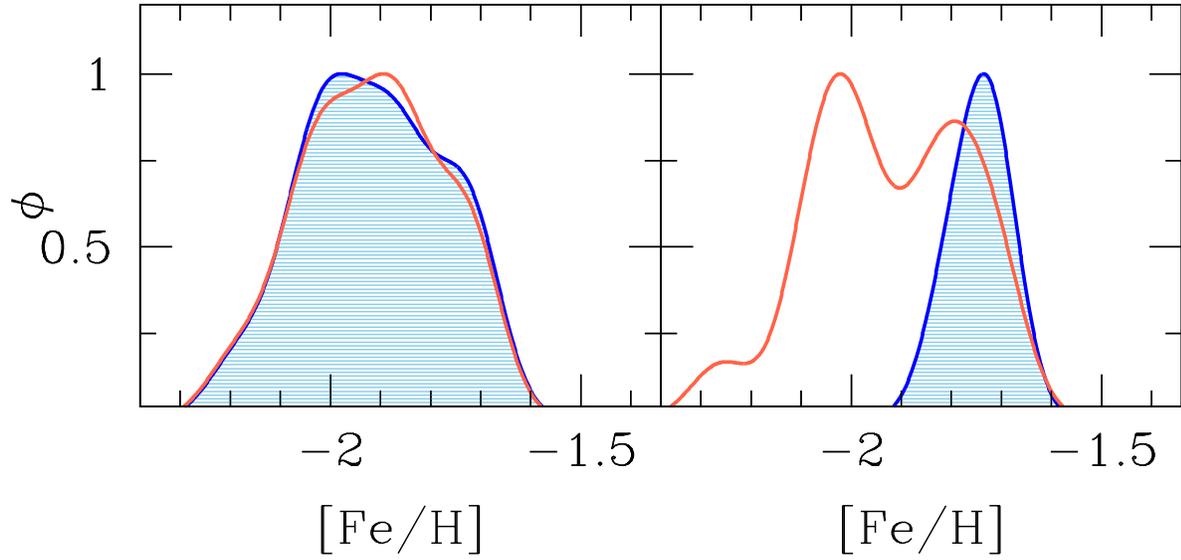
Fig. 2.— Generalized histograms for [FeI/H] (empty red histogram) and [FeII/H] (blue histogram) obtained from the analysis performed with spectroscopic gravities (method (1), left panel) and with photometric gravities (method (2), right panel).
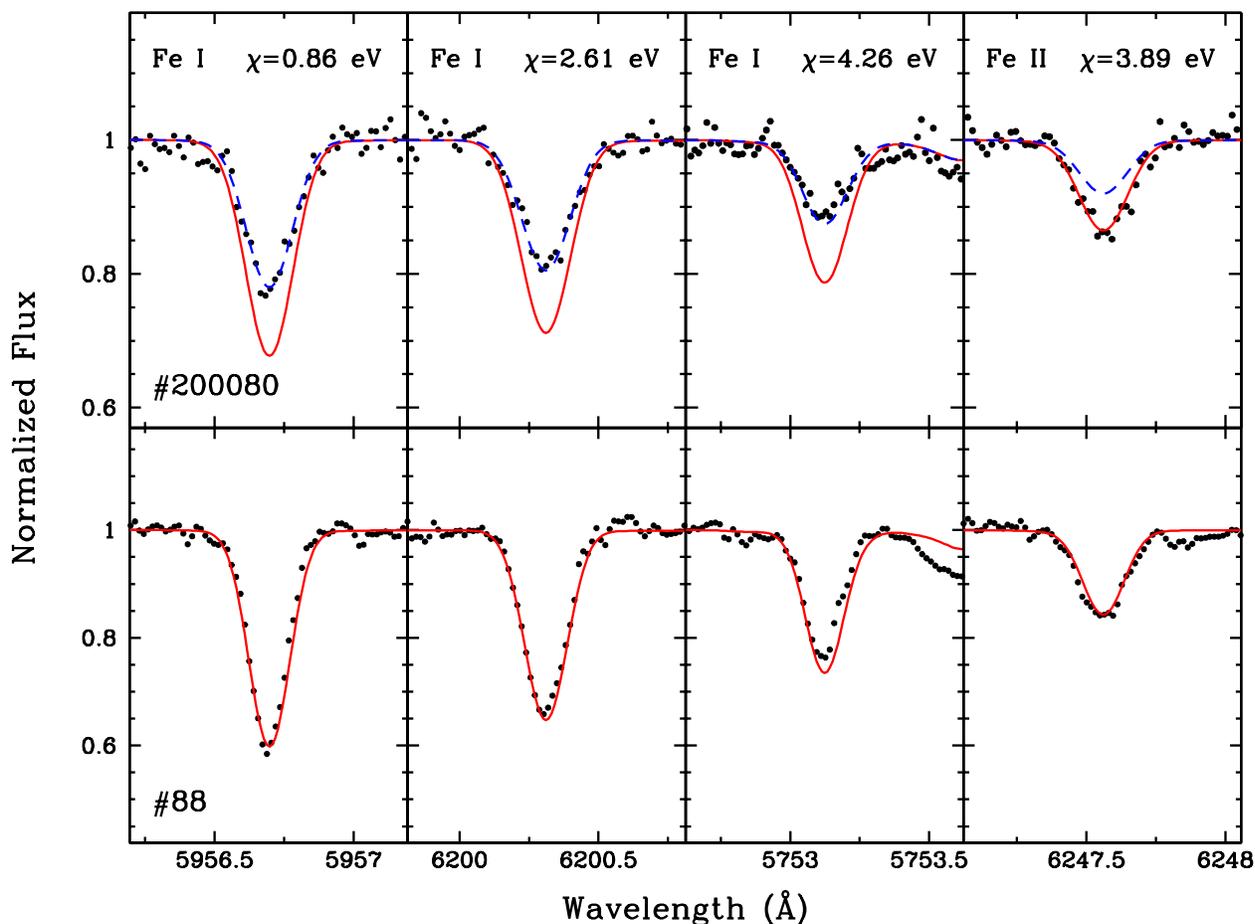
Fig. 3.— Spectral regions around three Fe I lines with different excitation potential and one Fe II line, for the target stars #200080 (upper panels) and #88 (lower panels). Synthetic spectra calculated with the corresponding atmospheric parameters (see Table 1) and adopting the average iron abundance derived from Fe II lines are superimposed as red curves. The blue dashed curve shown in the upper panels is the synthetic spectrum calculated with the iron abundance derived from Fe I lines.
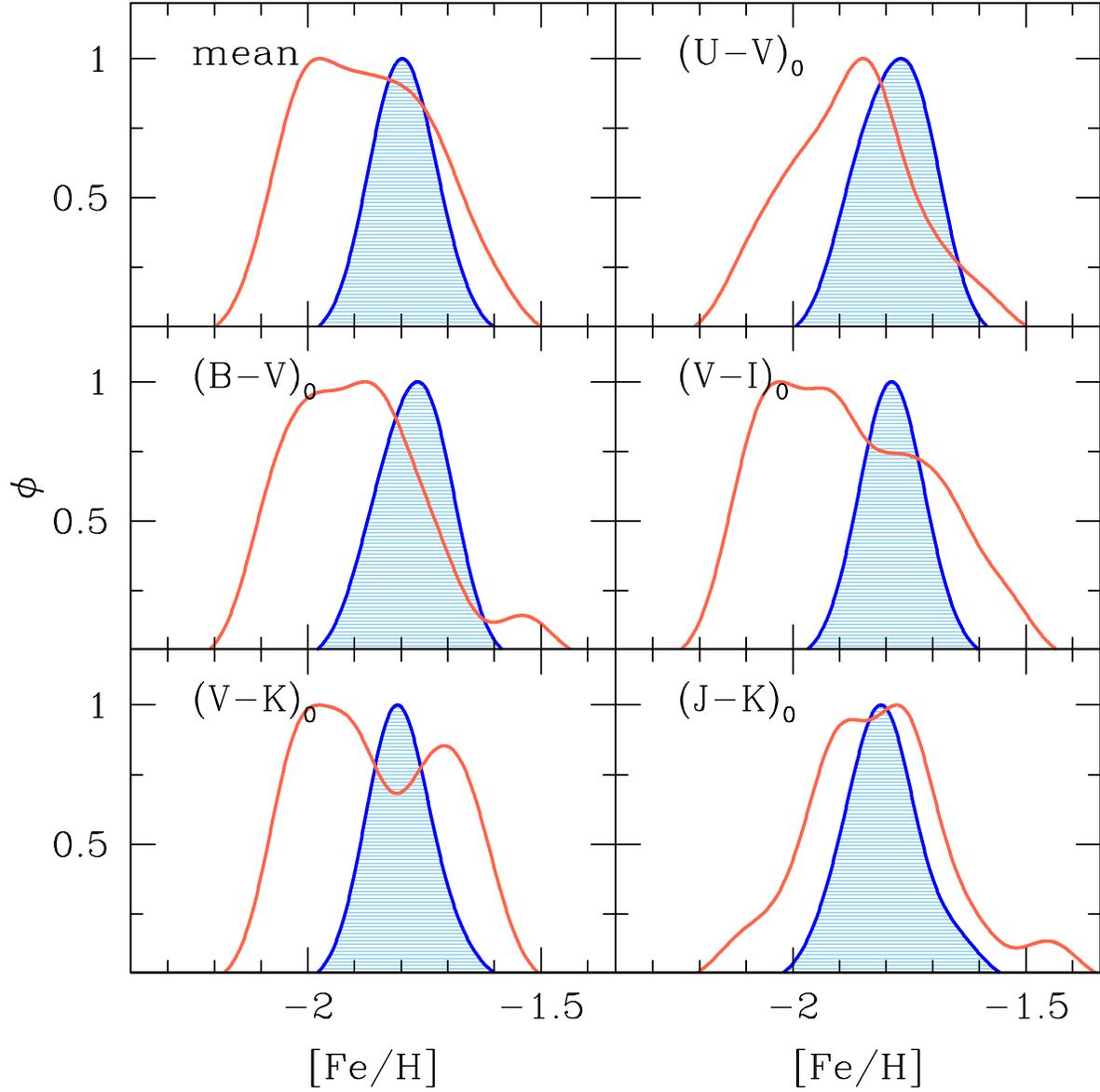
Fig. 4.— Generalized histograms for [FeI/H] and [FeII/H] (same colors of Fig. 2) obtained with the method (3) (photometric T_{eff} and log g), adopting the mean parameters (left-upper panel) and those derived from individual broad-band colors.
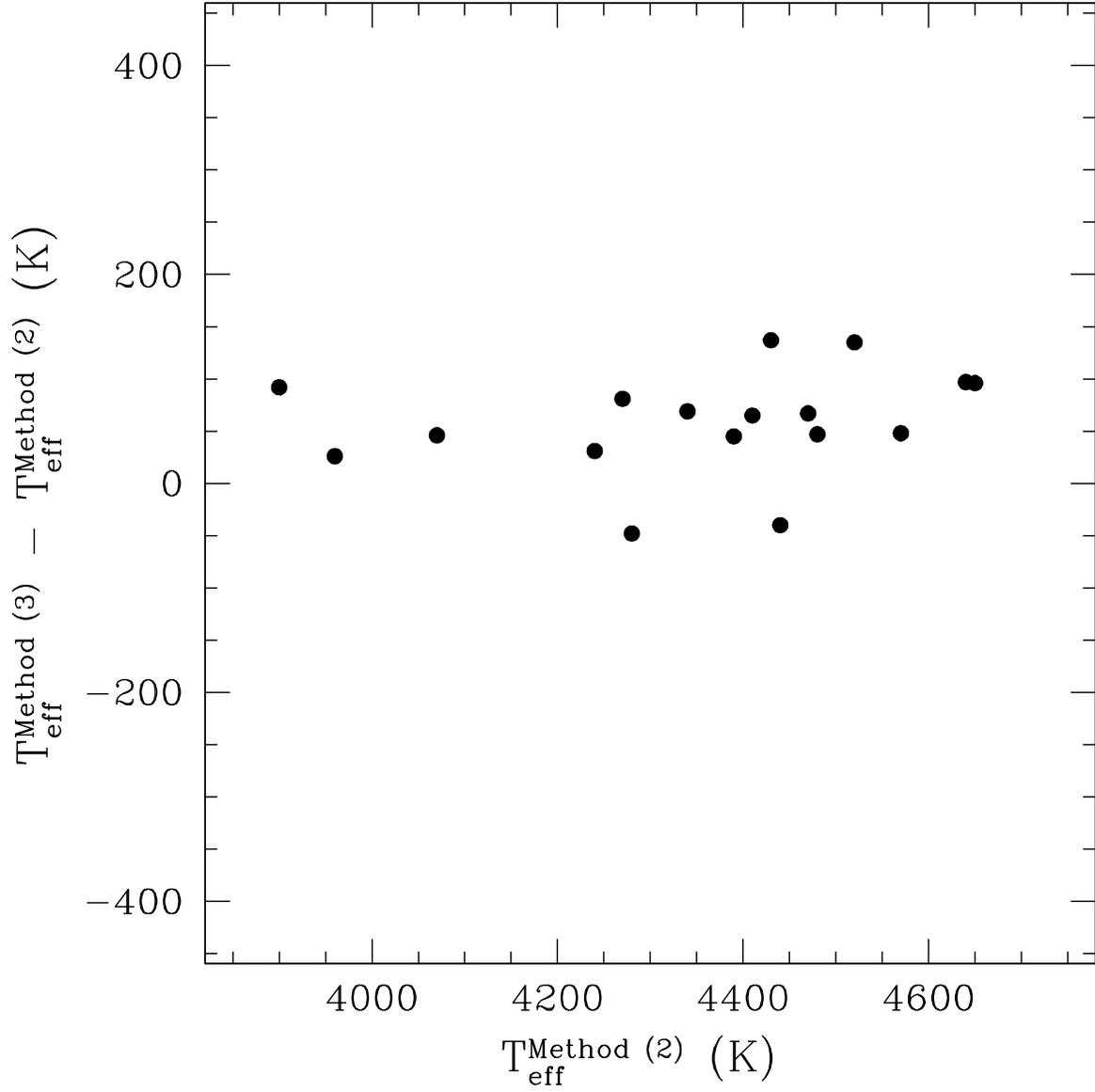
Fig. 5.— Behaviour of the difference between T_{eff} as derived with method (3) and (2) as a function of those derived with method (2).

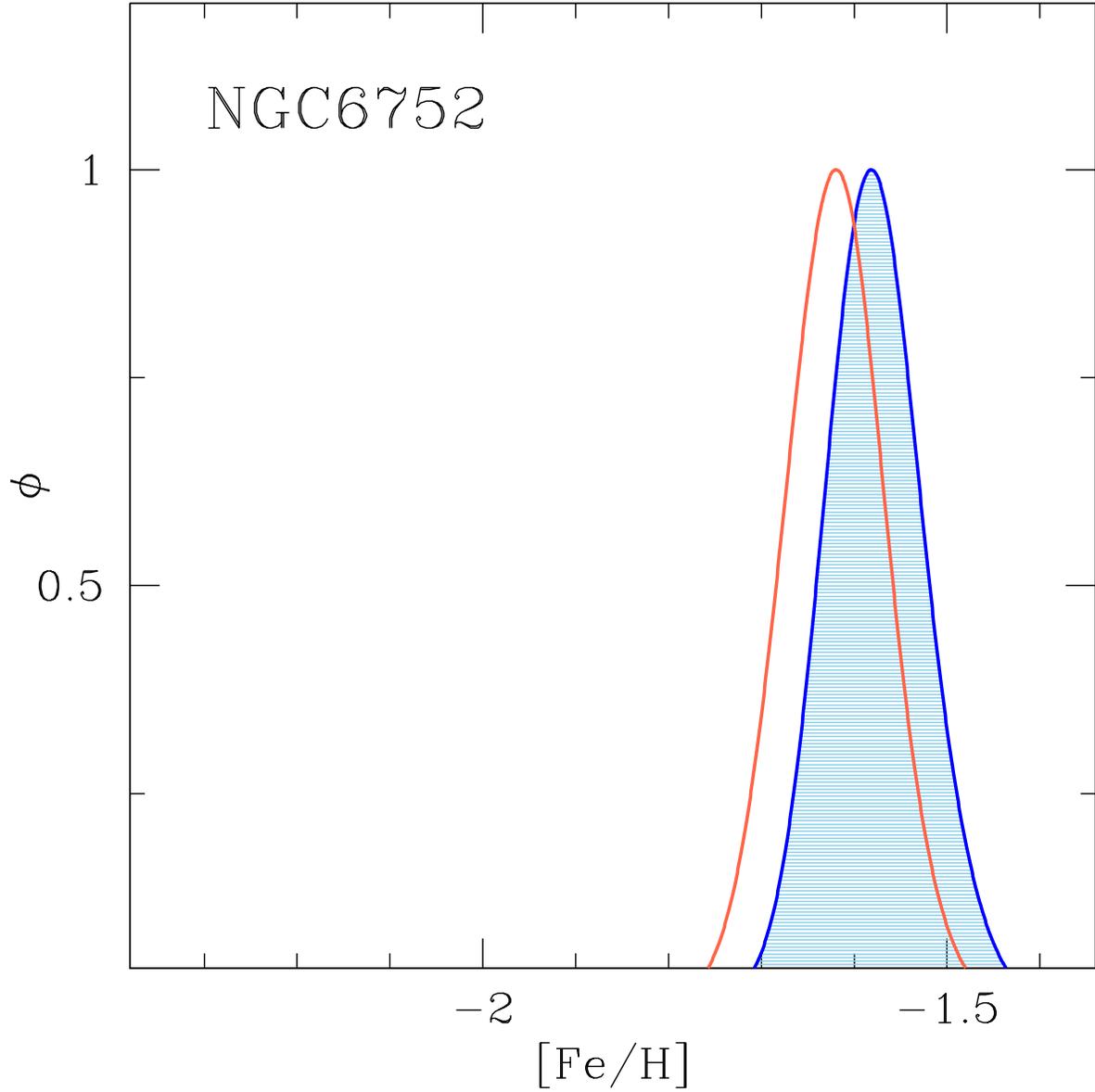Fig. 6.— Generalized histograms for [FeI/H] and [FeII/H] (same colors of Fig. 2) for a sample of 14 RGB stars in the GC NGC 6752. The analysis has been performed adopting spectroscopic T_{eff} and photometric log g, the same method used for the right panel of Fig. 2.
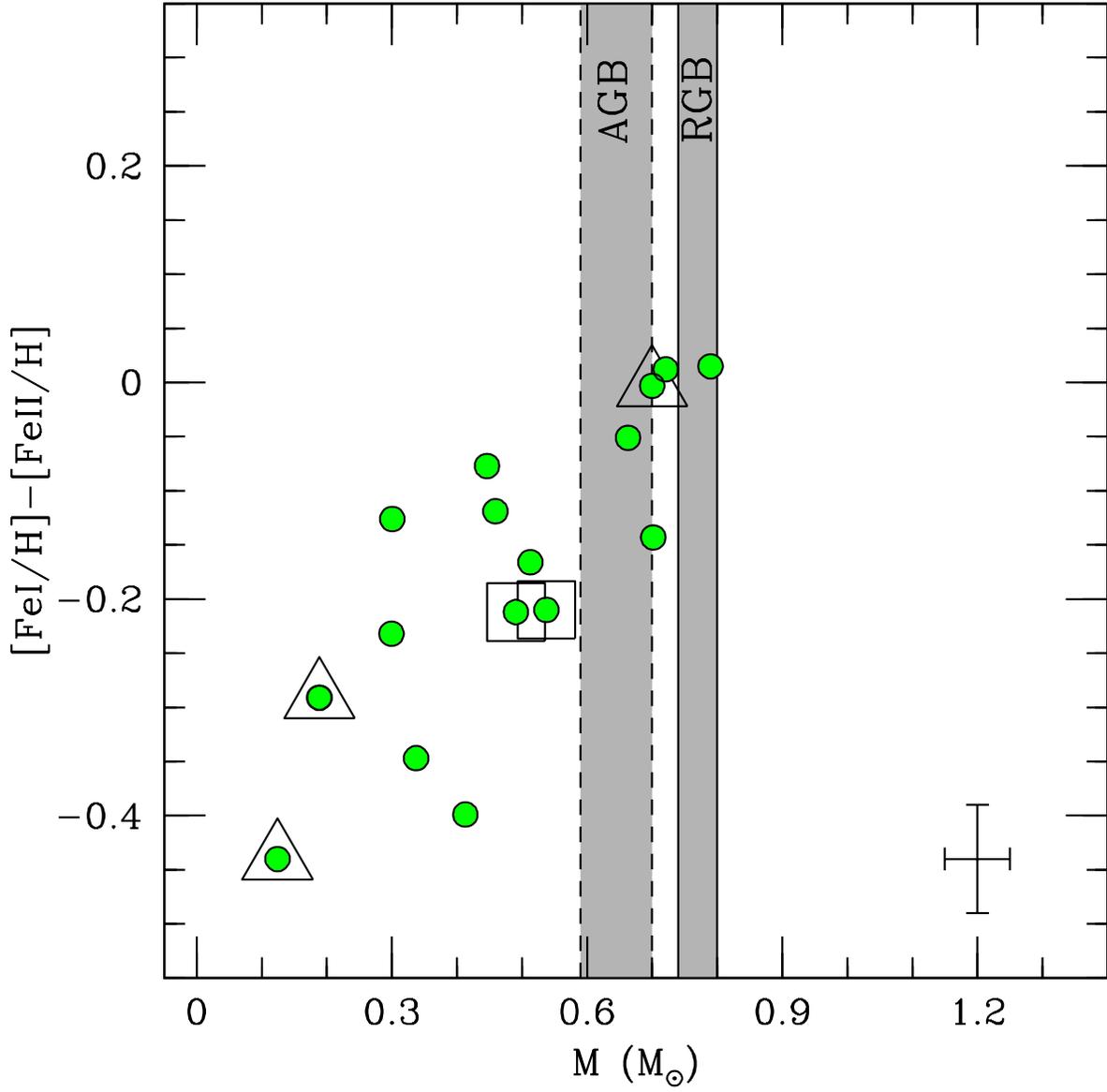
Fig. 7.— Behavior of the difference [FeI/H]-[FeII/H], as derived with method (2), of the spectroscopic targets as a function of the stellar masses inferred from the spectroscopic log g in method (1). The two shaded grey regions mark the mass range expected for AGB and RGB stars. Same symbols of Fig. 1.
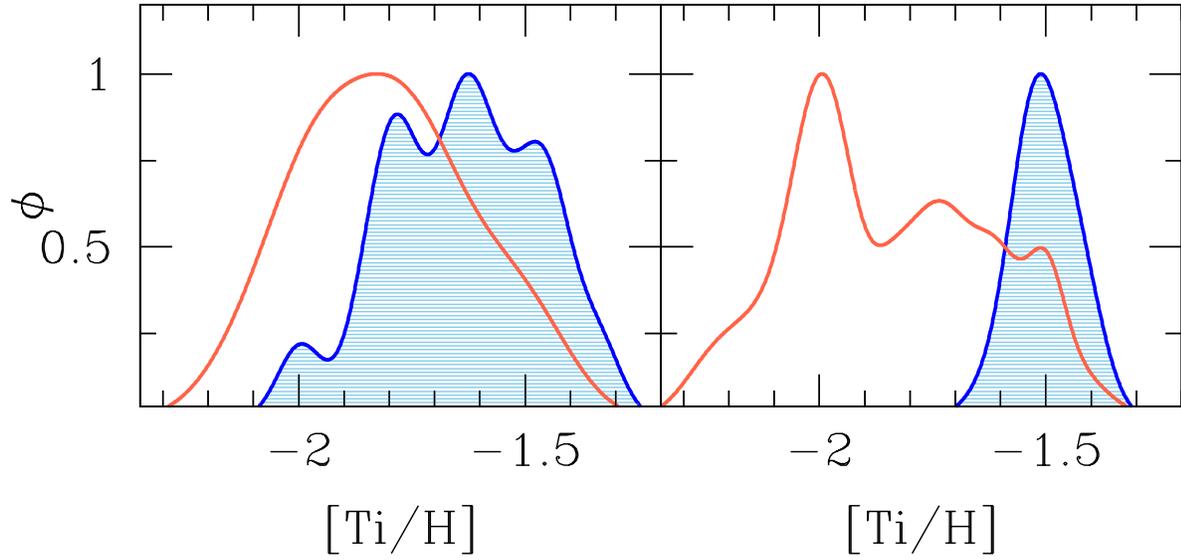
Fig. 8.— Generalized histograms for [TiI/H] (empty red histogram) and [TiII/H] (blue histogram) obtained adopting the spectroscopic (left panel) and photometric log g (right panel).
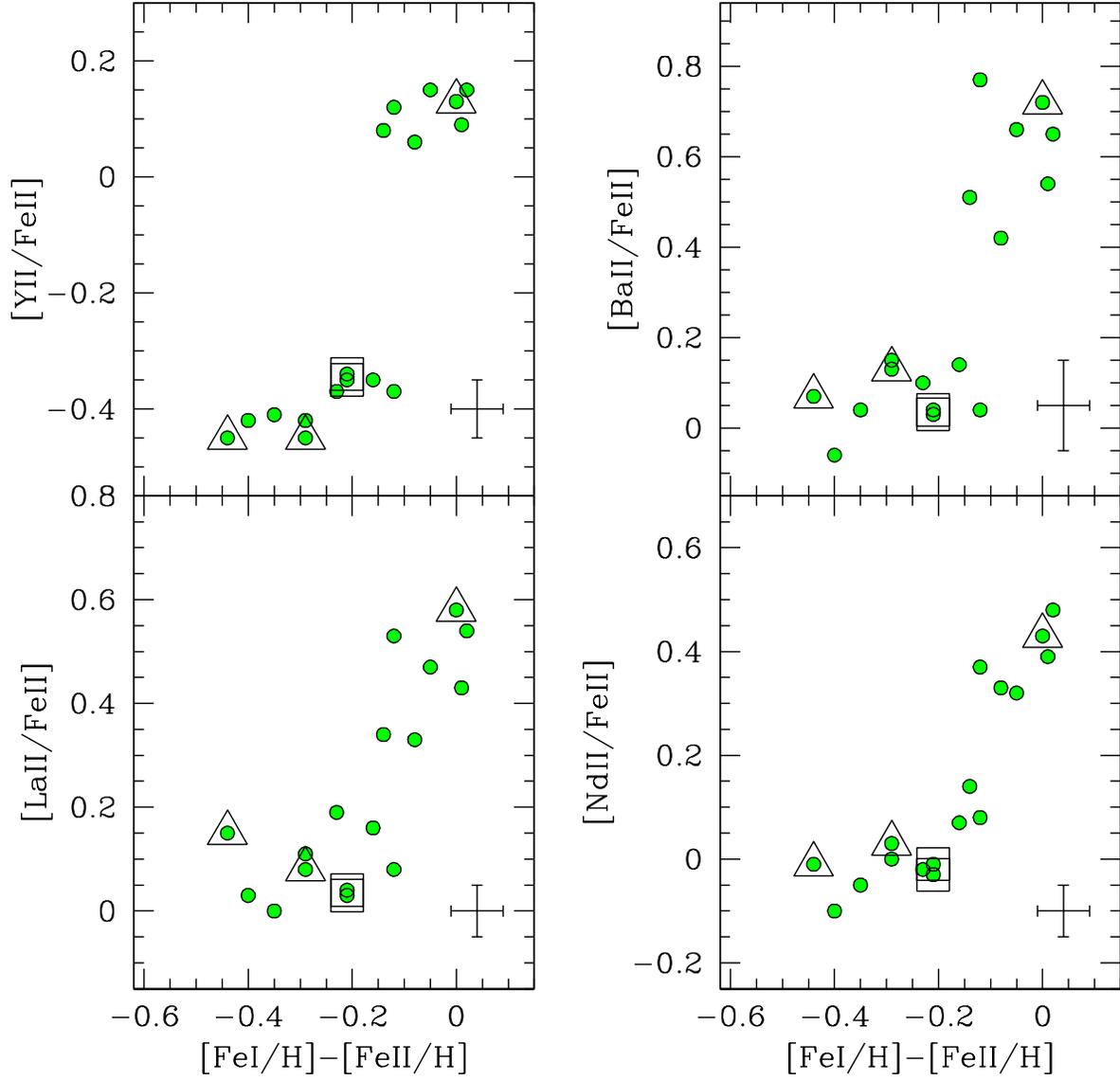
Fig. 9.— Behavior of the abundance of the s-process elements Y, La, Ba and Nd as a function of the difference between [FeI/H] and [FeII/H]. Same symbols of Fig. 1.
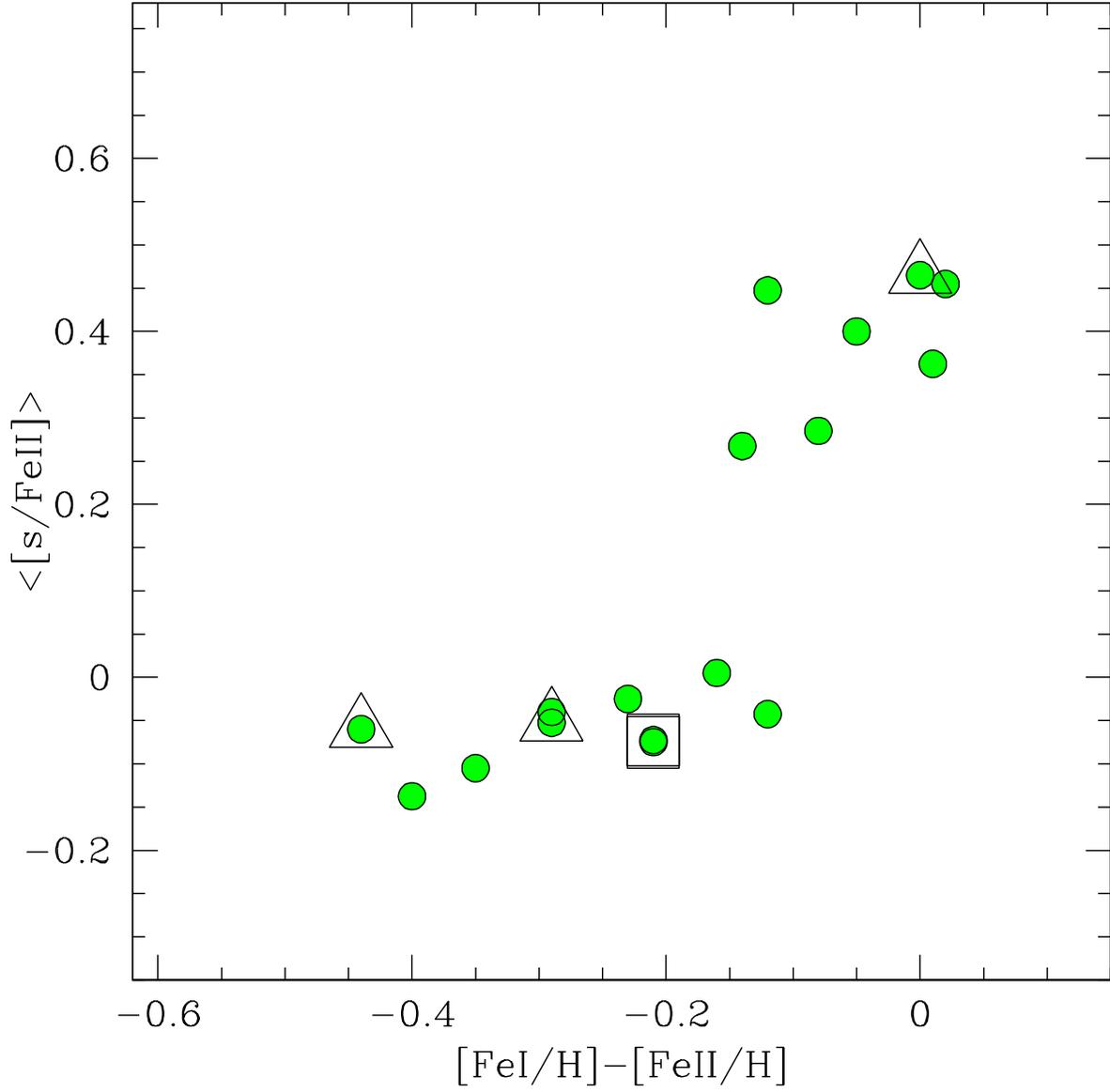
Fig. 10.— Behavior of the average abundance of s-process elements (derived by averaging together the abundances of Y, La, Ba and Nd) as a function of the difference between [FeI/H] and [FeII/H]. Same symbols of Fig. 1.